Engineering of Ferroelectric Switching Speed in Si Doped HfO_2 for High-Speed 1T-FERAM Application

H. K. Yoo[1], J. S. Kim[1], Z. Zhu[2], Y. S. Choi[1], A. Yoon[2], M. R. MacDonald[3], X. Lei[3], T. Y. Lee[4], D. Lee[5,6], S. C. Chae[4], J. Park[5,6], D. Hemker[2], J. G. Langan[3], Y. Nishi[7] and S. J. Hong[1]
[1]SK Hynix Inc., Icheon-si, Gyeonggi-do, Korea, email: hyangkeun.yoo@sk.com
[2]Lam Research Corp., Fremont, CA, USA; [3]Versum Materials, Carlsbad, CA, USA; [4]Dep. of Phys. Edu., Seoul Nat. Univ., Seoul, S. Korea; [5]CNR, Institute for Basic Science (IBS), Seoul, S. Korea; [6]Dep. of Chem. & Bio. Eng., Seoul Nat. Univ., Seoul, S. Korea; [7]Dep. of Elec. Eng., Stanford Univ., Stanford, CA, USA

***Abstract*—** Ferroelectric (FE) HfO_2 has a higher coercive field (E_c) than that of perovskite. High E_c guarantees a robust FE state, but it also implies a relatively slow switching speed under the same external field. Here, we propose a control of grain size in Si:HfO_2 which would lower the E_c, thereby, increase the switching speed. In order to achieve the goal, we studied and optimized Si-contents and post-anneal condition for nano-grain sized Si:HfO_2. We successfully demonstrated that Si:HfO_2 consists of controlled nano-grains with a FE property of E_c ~0.5MV/cm, which is a half of the ordinary Si:HfO_2, and the domain switching speed reaches ~3 times faster than that of ordinary grain sized Si:HfO_2. The domain dynamics is explained by the intrinsic domain-wall growth mechanism, which means no significant defect generations during the nano-grain formation.

1. Background and objective

FE HfO_2 has been recently discovered in the non-centrosymmetric orthorhombic phase [1]. Since HfO_2 based materials have already been used in CMOS technology for gate insulator, FE HfO_2 is considered as a material with better process compatibility, device scalability and performance as compared to that of perovskite [1]. It has attracted enthusiastic attention for new type of non-volatile memory applications including 1T-FERAM [1], 3D FENAND [2] and advanced neuromorphic computing devices [3]. Especially, for 1T-FERAM application, the FE domain switching speed should be compatible with the conventional DRAM or at least other new non-volatile memories. Intrinsic FE property is considered as the phonon mediated collective phenomena, which suggests the switching speed can be as fast as the speed of sound [4]. However, it is usually much slower in real materials due to extrinsic disorders [5]. Therefore, in HfO_2 based FE materials, understanding the switching mechanism and its characteristics should be definitely needed before practical device applications. Nevertheless, there have been no reported systematic investigations. Here, we investigated the switching speed of FE Si:HfO_2 as well as its governing mechanism.

II. Results and discussion

A. Sample growth and measurement details.

Si:HfO_2 was deposited on bottom TiN contact by ALD process based on TDMAH, 4DMAS and ozone, followed by top TiN deposition by CVD process and post-annealing in N_2 ambient to crystallize the Si:HfO_2 at 600°C for 20sec. The sample structure is 10nm TiN/8nm Si:HfO_2/10nm TiN as shown in Fig. 1(a). The diameter of the top electrode is 100 μm. To understand the mechanism of FE switching dynamics, we investigated the frequency (f) dependence of P-E hysteresis loop. In Fig. 2(a), we applied triangular waves with various f (i.e. 10Hz~50kHz) to the Si:HfO_2 capacitors by using a TF analyzer 3000 (aixACCT). Additionally, in Fig. 2(b), we applied a square-pulse with various amplitudes (i.e. 0.9~3.8MV/cm) and widths (140ns~1ms) to estimate the FE switching speed.

B. FE domain dynamics of optimally Si doped HfO_2

Figure 1(b) reveals P-E curves of Si 4.2 mol% doped HfO_2 (4.2Si:HfO_2) in as-grown and after-cycles. We used a dynamic hysteresis measurement function in TF-3000 with 1kHz, 3V amplitude. The as-grown sample shows a small imprint into a negative direction. We assumed that this could originate from the trapped pinning sites due to charged defects such as oxygen vacancies which is generated during the top TiN growth. After 10^4-cycle operation, the P-E curve becomes symmetric with remnant polarization P_r~20uC/cm^2 and E_c~1MV/cm. These values are consistent with previous reports of the optimally doped Si:HfO_2 [1]. Additionally, in our results, the 4.2Si:HfO_2 sample shows the largest P_r, so we concluded that this is the nearly optimal-doped sample.

The switching dynamics of the FE 4.2Si:HfO_2 can be explained by the domain-wall growth mechanism. In Figs. 3(a) and (b), we measured f dependence of P-E hysteresis loops in as-grown and after-cycles. When the f increases from 10Hz to 50kHz, the E_c increases. The $E_{c\pm}$ versus f curves are depicted in Figs. 4(a) and (b). We found that the E_c is proportional to log f with two-scaling regions corresponding to creep and flow motions in the domain-wall growth model [6] independent of cycling conditions. This result indicates that the FE domain dynamics in the 4.2Si:HfO_2 is governed by intrinsic domain-wall motion, not an extrinsic defects-driven one [5].

The switching speed of FE domain in 4.2Si:HfO_2 is limited by a large E_c. We measured the pulse time (t)-dependent change in polarization $\Delta P(t)$ by varying the amplitudes of the applied external fields (E_{app}) from 0.9 to 3.8MV/cm. The $\Delta P(t)$ normalized by 2 times of saturated polarization P_s versus log t graphs are shown in Figs. 5(a) and (b). When the E_{app} increases, the switched $\Delta P(t)/2P_s$ starts increasing at the same pulse t.

However, we found that the switched $\Delta P/2P_s$ with 100ns pulse [ΔP(100ns)] is less than 30% even with high E_{app}, 3.8MV/cm. In the FE domain-wall growth model, switching speed strongly depends on E_c [7]. The E_c of the 4.2Si:HfO_2 is ~1MV/cm which is 10~100 times larger than that of perovskite-based FE materials [8]. This is likely the origin of slow switching speed, so the controllability of E_c is one of the prerequisites for high-speed FE device development including 1T-FERAM.

C. Si doping level dependence upon FE properties of HfO_2

We varied the Si-contents between 2.3 and 5.7mol%. Note that, for 5.7Si:HfO_2, we used 800°C for 10sec. to crystallize the highly Si-doped HfO_2 [9]. In Fig. 6(a), the XRD data of the 4.2Si:HfO_2 shows a dominant orthorhombic peak, whereas 2.3 and 5.7Si:HfO_2 samples reveal the additional monoclinic and tetragonal peaks. In Fig. 6(b), the 2.3Si:HfO_2 sample shows a strong imprint into a negative direction and still remains after-cycles. The 5.7Si:HfO_2 sample shows an anti-FE like behavior due to tetragonal phase [10] (not shown here).

We investigated the FE switching dynamics in the mixed phases of HfO_2. The switching dynamics of the 2.3Si:HfO_2 can be explained by a nucleation-limited-switching mechanism. The *f* dependence of *P-E* hysteresis loop and the $E_{c\pm}$ versus *f* curves for as-grown and after-cycles are shown in Figs. 7 and 8. The E_c becomes gradually increased when the *f* increases and it does not show a clear two-scaling regions. This behavior is similar to the defect-driven nucleation-limited FE switching [5]. The *P-E* curves strongly depend upon cycling which could originate from the change of the internal phase configurations [10]. Additionally, we measured the $\Delta P(t)/2P_s$ versus log *t*. Note that we performed the experiments with both write square-pulse directions due to large imprint. The $\Delta P(t)/2P_s$ show strong dependence on the square-pulse direction and the cycle numbers as shown in Figs. 9 and 10. Our results indicate that the defect driven FE switching has large variability, which is difficult to control and utilizes in device applications.

D. FE domain dynamics of nano-grain HfO_2

The requirement to achieve the fast switching property in the FE Si:HfO_2 is to lower the E_c without unwanted disorder effects. However, the conventional methods such as doping control to tune the E_c always introduce the unavoidable disorder effects. Alternatively, when the crystal size is reduced toward the critical size for FE as shown in Fig. 11(a), the FE property becomes less stable with decreasing switching barrier [11]. This, on the contrary, suggests that HfO_2 grain size reduction can be a new avenue to lower the E_c for faster switching without significant defect generations.

The crystallization of Si:HfO_2 is sensitive to the Si-contents and post-annealing temperature [9]. Figure 12(a) shows a phase diagram of Si:HfO_2. We found that the grain size of Si:HfO_2 ranges from tens-of-nm to ~0 nm at which point the phase boundary crosses over from crystalline to amorphous. We held the post-annealing temperature constant at 600°C. The crystallization succeeds up to the Si 4.2 mol% concentration, whereas it fails in crystalizing at the higher % of 5.7 and 7.3 Si:HfO_2 samples. The crystallization states are measured by the XRD [Fig. 12(b)]. In Fig. 13 of TEM results, the grain size of the 4.2Si:HfO_2 is sub-20nm, whereas that of 5.7Si:HfO_2 is not observed in our TEM measurement with sub-1nm spatial resolution. The Figure 14(a) reveals *P-E* curves of as-grown and after-cycled 5.7Si:HfO_2. The as-grown sample shows a small anti-FE like *P-E* curve. However, after cycles, the *P-E* curve becomes symmetric. Based on the XRD, TEM and *P-E* results, we conclude that the 5.7Si:HfO_2 consists of nano-grains of FE orthorhombic phase with low E_c.

The switching dynamics of the FE 5.7Si:HfO_2 can be explained by the intrinsic domain-wall growth mechanism. In Figs. 15 and 16, the E_c is proportional to log *f* with two-scaling regions consistent with the results of FE 4.2Si:HfO_2. The two-scaling behavior is also independent on cycling conditions. This result supports that making the nano-grain of FE Si:HfO_2 is not accompanied by significant defect generations. Additionally, we also measured the $\Delta P(t)/2P_s$ versus log *t* by varying the cycle numbers. In Fig. 17, we found that the amount of the switched $\Delta P(t)/2P_s$ is enlarged by reduction of E_c. With 0.44 and 0.55 MV/cm of E_c, the switched ΔP(100ns) becomes ~80% and ~65% with 3.8MV/cm of E_{app}, respectively.

Figure 18(a) reveals the switching time for 80% $\Delta P/2P_s$ versus E_c curves by varying the E_{app} from 2.0 to 3.8MV/cm. The E_c values are extracted by *P-E* curves in Fig. 14. It clearly demonstrates the reduced switching time by lowering the E_c. Figure 18 (b) shows the universal domain switching dynamics in defect-free FE Si:HfO_2. We extracted ΔP(500ns) values and normalized the E_{app} by each E_c for three different cases. ΔP(500ns) versus E_{app}/E_c follows the same curve. We concluded that FE switching dynamics of defect-free Si:HfO_2 is governed by the same domain-wall growth mechanism independent of the grain size and E_c values.

III. Conclusion

Though it has been a common knowledge that large coercive field, E_c, limits the FE switching speed of Si:HfO_2, we successfully made Si:HfO_2 films consisting of nano-grains, resulting in much lower E_c. Our experimental data proved that the FE switching speed can be enhanced by grain size control without unwanted disorder effects. Our results provide a new way how to realize the high speed FE switching devices including 1T-FERAM.

ACKNOWLEDGMENT

The authors gratefully acknowledge the contributions of all of joint development (JD) members in Lam Research, Versum Materials and SK Hynix. J. P. and D. L. acknowledges support by IBS-R001-D1.

REFERENCES

[1] J. Muller *et al.*, IEDM 10.8.1 (2013). [2] K. Florent *et al.*, VLSI T12-4 (2017). [3] H. Mulaosmanovic et al., VLSI T13-3 (2017). [4] D. S. Rana *et al.*, Adv. Mater. **21**, 2881 (2009). [5] D. J. Jung *et al.*, Integr. Ferroelectr. **48**, 59 (2002). [6] S. M. Yang *et al.*, Phys. Rev. B **82**, 174125 (2010). [7] J. Y. Jo *et al.*, Phys. Rev. Lett. **102**, 045701 (2009). [8] J. Mller *et al.*, ECS J. Solid State Sci. Tech. **4**, N30 (2015). [9] E. Yurchuck *et al.*, Thin Solid Films, **533**, 88 (2013). [10] M. Pešić *et al.*, Adv. Func. Mater. **26**, 4601 (2016). [11] J. Junquera and P. Ghosez, Nature 422, 506 (2003). [12] J. Y. Jo *et al.*, Phys. Rev. Lett. **99**, 267602 (2007).

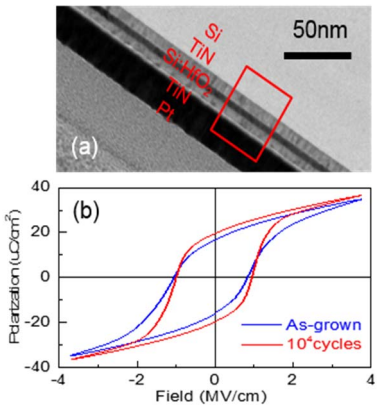

Fig. 1. (a) TEM image of Si:HfO_2 capacitor, (b) *P-E* hysteresis loop for 4.2 mol% Si:HfO_2 in as-grown and after-10^4 cycles.

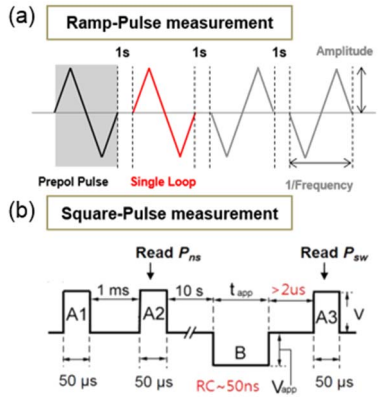

Fig. 2. Sequences of (a) ramp-pulse measurement dependent on frequency and (b) Square-pulse measurement dependent on t_{app} and write pulse voltage, V_{app}.

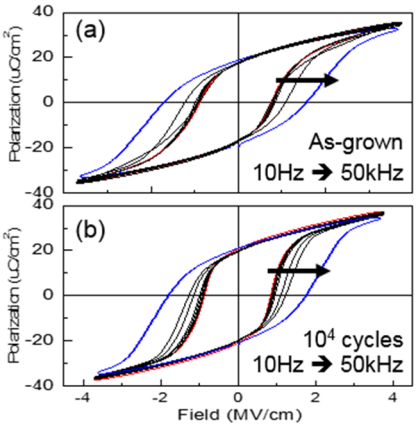

Fig. 3. Frequency dependence of *P-E* hysteresis loop of (a) as-grown and (b) 10^4-cycled 4.2 mol% Si:HfO_2. We performed the measurement by increasing frequency from 10Hz to 50 kHz.

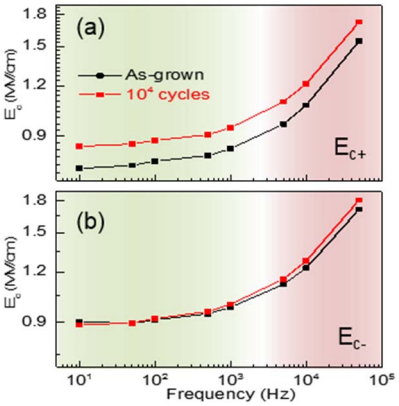

Fig. 4. (a) E_{c+} and (b) E_{c-} versus frequency curves in as-grown and 10^4-cycled 4.2 mol% Si:HfO_2. Green and red areas are corresponding to creep and flow regimes.

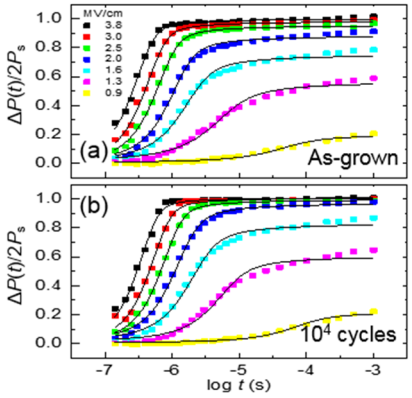

Fig. 5. Time-dependent change of polarization, $\Delta P(t)$, by varying the amplitudes in (a) as-grown and (b) 10^4-cycled 4.2 mol% Si:HfO_2. The solid lines are fitting results [12]. Write pulse (E_{app}) is in the negative direction.

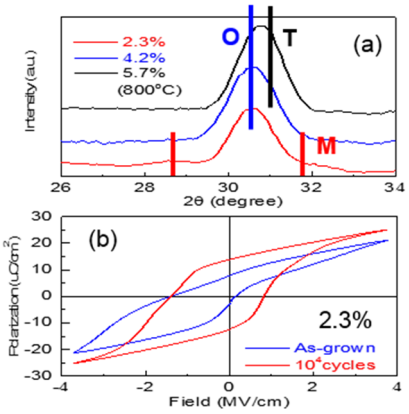

Fig. 6. (a) XRD data of various Si doped HfO_2. Peaks are assigned by orthorhombic (O), tetragonal (T), and monoclinic (M) phases. (b) *P-E* hysteresis loop for 2.3 mol% Si:HfO_2 in as-grown and after-10^4 cycles.

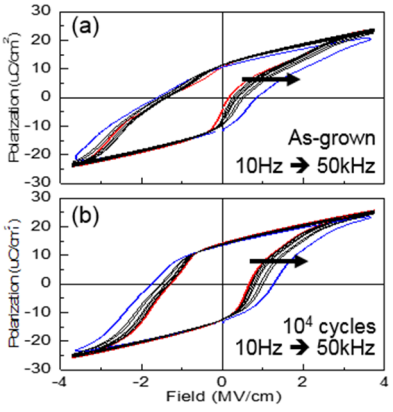

Fig. 7. Frequency dependence of *P-E* hysteresis loop of (a) as-grown and (b) 10^4-cycled 2.3 mol% Si:HfO_2. We performed the measurement by increasing frequency from 10Hz to 50 kHz.

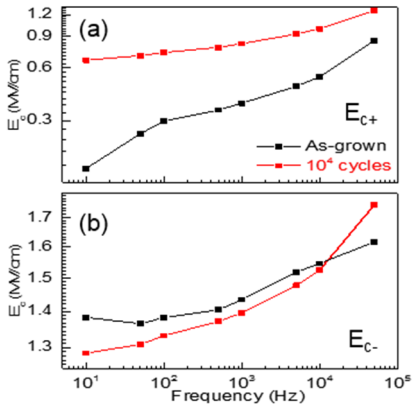

Fig. 8. (a) E_{c+} and (b) E_{c-} versus frequency curves in as-grown and 10^4-cycled 2.3 mol% Si:HfO_2.

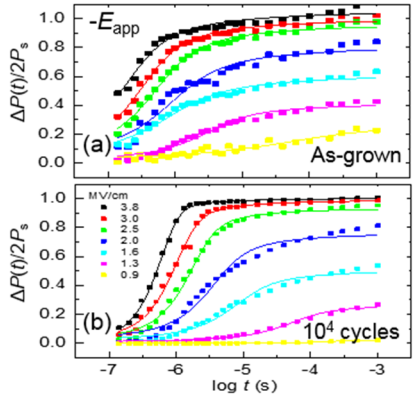

Fig. 9. Time-dependent change of polarization, $\Delta P(t)$, by varying the amplitudes in (a) as-grown and (b) 10^4-cycled 2.3 mol% Si:HfO_2. Write pulse (E_{app}) is in the negative direction.

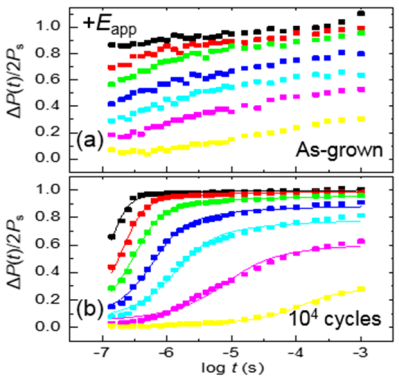

Fig. 10. Time-dependent change of polarization, $\Delta P(t)$, by varying the amplitudes in (a) as-grown and (b) 10^4-cycled 2.3 mol% Si:HfO_2. Write pulse (E_{app}) is in the positive direction.

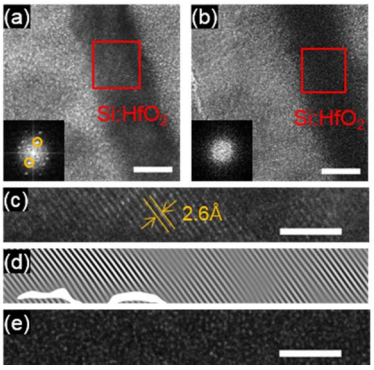

Fig. 13. TEM images of (a) 4.2, (b) 5.7% Si doped HfO_2, respectively. Si doped HfO_2 films are in dark contrast embedded between top and bottom TiN electrodes. Scale bars 5nm. Insets are FFT patterns of red-squared region of each image. (c) Magnified TEM image of HfO_2 film with 4.2% Si doping. Scale bar 3nm. (d): Inverse FFT of (c) filtered by selected bright spots (orange color in (a)) of inset in (a). (e) Magnified TEM image of HfO_2 film with 5.7% Si doping. Scale bar 3nm.

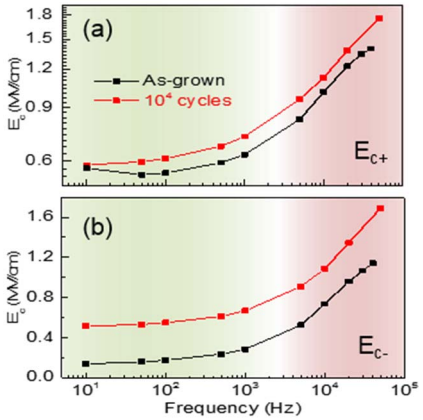

Fig. 16. (a) E_{c+} and (b) E_{c-} versus frequency curves in as-grown and 10^4-cycled 5.7 mol% Si:HfO_2. Green and red areas are corresponding to creep and flow regimes.

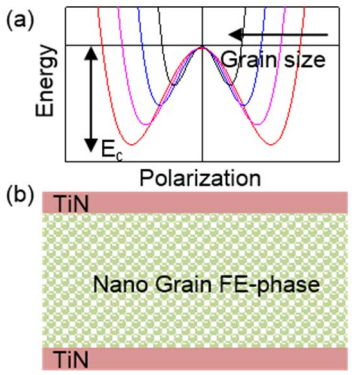

Fig. 11. (a) Simple schematic of double-well potential dependent on the grain size, (b) Schematic of Si:HfO_2 film consisting of FE O-phase nano-grains

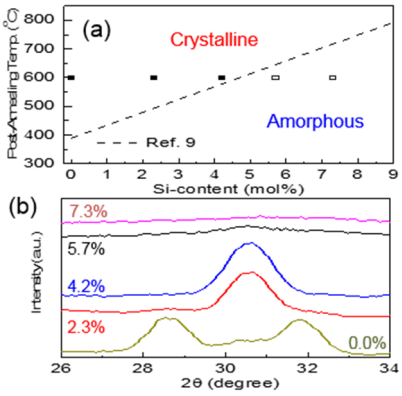

Fig. 12. (a) Phase map of crystallization in Si:HfO_2 dependent on the Si-contents and post-annealing temperature, (b) XRD data of various as-grown Si doped HfO_2 samples marked in (a).

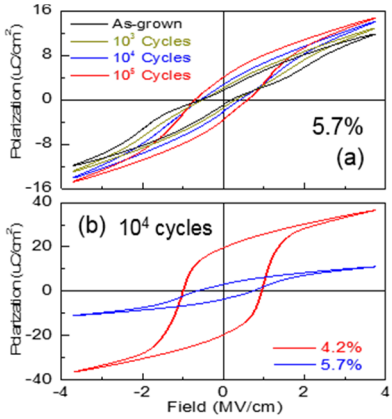

Fig. 14. (a) *P-E* hysteresis loops for 5.7 mol% Si:HfO_2 by varying the cycles, (b) Comparison between *P-E* curves of 4.2 and 5.7 mol% Si:HfO_2 after 10^4 cycles.

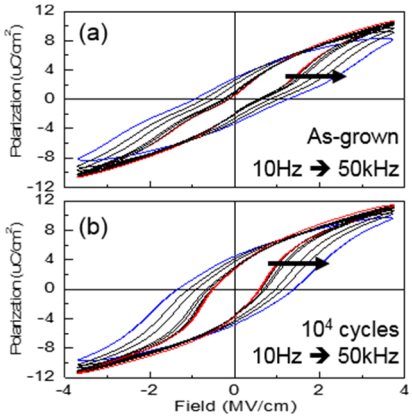

Fig. 15. Frequency dependence of *P-E* hysteresis loop of (a) as-grown and (b) 10^4-cycled 5.7 mol% Si:HfO_2. We performed the measurement by increasing frequency from 10Hz to 50 kHz.

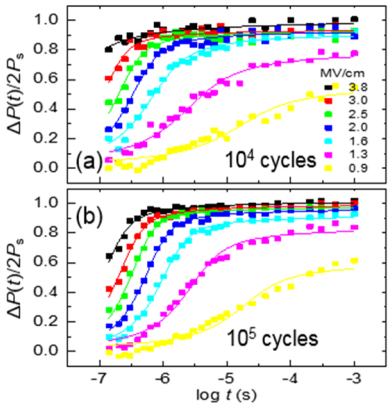

Fig. 17. Time-dependent change of polarization, $\Delta P(t)$, by varying the amplitudes in (a) as-grown and (b) 10^4-cycled 5.7 mol% Si:HfO_2. Write pulse (E_{app}) is in the negative direction.

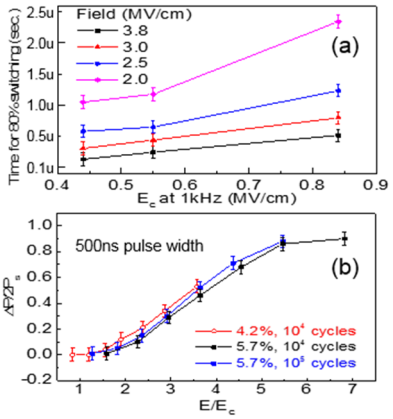

Fig. 18. (a) Switching time for 80% polarization change versus the coercive field E_c by varying the external field. (b) Polarization changes with 500ns pulse versus the external field normalized by the coercive field E_c. The three different cases are in the same curve.